THE ASTRONOMICAL JOURNAL VOLUME 105, NUMBER 1 JANUARY 1993

THE RADIO PROPERTIES OF CD GALAXIES IN ABELL CLUSTERS. II. THE VLA SAMPLE[1]

RAYFORD BALL, JACK O. BURNS, AND CHRIS LOKEN
Department of Astronomy, Box 30001/Department 4500, New Mexico State University, Las Cruces, New Mexico 88003

Received 6 July 1992; revised 15 September 1992

ABSTRACT

The radio properties of a sample of 91 cD galaxies in Abell clusters are presented. The radio data consist of new 6 cm VLA maps with a resolution of 1″–2″ as well as data from the literature. The principal goal of this project was to investigate the possible effects of global and local cluster properties on the radio properties of cDs. The dominant predictor of central radio activity is the presence of x-ray cooling flows, as reported in Paper I [Burns, J. O., AJ, 99, 14 (1990)]. Results described in this paper indicate a slight increase in the detection rate and a steeper spectral index for cDs in Bautz–Morgan (B–M) I clusters in comparison to clusters having any other B–M type. Cluster richness and cD absolute magnitude seem to be uncorrelated with radio power. However, there is a possible weak correlation of radio power with the ellipticity of the cD at 16 kpc from the galaxy's optical center. The radio morphological types of the detected galaxies are related to radio-luminosity and spectral index with compact radio sources being most often detected. Steep-spectrum, amorphous sources are a peculiar class of radio source associated exclusively with dominant galaxies in cooling flows. Finally, a 6 cm radio luminosity function (RLF) is computed for cDs and compared to the RLF for cluster galaxies in general. Interestingly, the slope of the RLF below the knee is flatter than that for other cluster ellipticals, possibly reflecting the unique environment and evolution of cDs.

1. INTRODUCTION

cD galaxies are defined (Mathews *et al.* 1964) as very luminous elliptical galaxies surrounded by an extended amorphous halo of low surface brightness. These galaxies are often found at the centers of regular, compact clusters of galaxies (Sarazin 1988). cDs are among the most luminous galaxies known. Their optical luminosity function is not a simple extrapolation of the bright end of the normal elliptical galaxy luminosity function but, rather, is a distinct function (Sandage 1976; Tremaine & Richstone 1977; Dressler 1978a).

Several theories have been proposed for the formation of cDs, based on their unusual structural and kinematic properties. Gallagher & Ostriker (1972) and Richstone (1975, 1976) proposed that cDs form as a result of galaxy interactions, and the outer halos of galaxies were tidally stripped to provide the material composing the cD. This model of cD formation might imply high velocity dispersions within cD halos, as has been observed in A2029 by Dressler (1979). Ostriker & Tremaine (1975), Gunn & Tinsley (1976), and White (1976, 1977) suggested that cDs are formed by the merger of massive galaxies within the core of a cluster, forming a single supergiant galaxy. This "cannibal galaxy" would then swallow any galaxies that would pass through the cluster center. If the cannibalism theory is correct, mergers should occur in a cluster about every 10^9 years. The actual merger process should require approximately one orbital period in the cD, about 3×10^9 years. During this time, the merging galaxy should be visible within the cD. Therefore, about one fourth of the observed cDs should have multiple nuclei, as has been observed (Hoessel 1980). However, some of these multiple nuclei have rather large velocities relative to the cD (Tonry 1985), suggesting that they are on highly elliptical orbits.

Merritt (1983, 1984a,b, 1985) pointed out some serious problems with these theories of cannibalism and tidal stripping for cD formation. He stated that some of the assumptions of cannibalism theory were poorly chosen. The large growth rate of the cannibal predicted by Hausman & Ostriker (1978) assumes that galaxies in clusters are surrounded by massive halos of dark matter. However, the tidal field resulting from the distributed matter in a cluster would probably truncate the halos of galaxies (Merritt 1984a; White 1983). Also, Merritt warned that if cluster galaxy masses are small, capture times for galaxies *initially* in the core would be comparable to a Hubble time. Merritt (1984a) reported the results of model calculations of this capture process, indicating a capture rate of essentially zero. He concluded that the essential properties of cD galaxies must be determined before cluster collapse. If cD galaxies are special, the dynamical processes that gave them their unique properties must have occurred early in the formation process.

The core of a rich cluster is a very active environment in which many other physical processes may be important. X-ray observations suggest that cDs are accreting vast amounts of gas. cDs tend to be radio-loud more often than typical nondominant cluster ellipticals (Burns *et al.* 1981; Bijleveld & Valentijn, 1983). The clusters in which they reside tend to be the most x-ray luminous class of clusters

[1]Observations reported in this paper were performed at the National Radio Astronomy Observatory which is operated by Associated Universities, Inc., under cooperative agreement with the National Science Foundation.

 0004-6256/93/010053-14$00.90

between 2 and 10 keV. In addition, the x-ray emission is always centered on the cD, suggesting that the cD is at the center of the gravitational potential well (Sarazin 1988).

About one third of the cDs observed by Jones & Forman (1984) to be x-ray sources have central radiative cooling times less than a Hubble time. As the central gas in the cluster cools, the core pressure drops. The higher gas pressure in the outer parts of the cluster will then drive a flow of gas into the core region. This cooling flow is thought to produce the excess x-ray surface brightness in the center of the cluster (Fabian *et al.* 1991). Edge & Stewart (1991) reported a sample of galaxy clusters, observed with the *EXOSAT* observatory, that exhibit cooling flows to some extent in about 90% of their cores. The implication is that cooling flows are a common phenomenon and are not a brief phase in the galactic evolution process (Edge & Stewart 1991).

The relationship between cooling flows and radio emission is still unclear. Based on *Einstein* x-ray data and single-dish radio data, Jones & Forman (1984) suggested a strong correlation between radio emission and cooling flows. However, O'Dea & Baum (1986) found only a weak correlation between 20 cm radio emission and excess central x-ray luminosity in cooling core clusters. Zhao *et al.* (1989) found a weak correlation between radio emission and cooling core clusters, based upon 20 cm data from the VLA and *Einstein* x-ray data.

Burns (1990) in Paper I used a subset of the data reported in this paper (27 cDs in rich clusters which also were observed by the *Einstein* IPC) to investigate the relationship between the x-ray and the 6 cm radio emission. No correlation between x-ray luminosity and 6 cm radio power was found. However, Burns (1990) did detect a strong relationship between the presence of x-ray cooling inflows and 6 cm radio emission. 71% of those cDs with cooling flows are radio-loud while only about 23% of those cDs without cooling flows produce detectable radio emission. Also, Paper I reported that sources with cooling flows are found to have steeper radio spectra.

This paper reports additional VLA observations of a larger sample of cDs in Abell clusters at 6 cm combined with data from the literature. Radio images at 6 and 20 cm, and optical data are analyzed. The goal of this project is to uncover relationships between 6 cm radio power and other measurable (and sometimes unique) properties related to these supergiant galaxies. The presence of cooling flows seems to be a predictor of radio emission (Burns 1990). However, other factors such as the optical luminosity, separation between "nuclei," cluster richness, or Bautz–Morgan type may also be related to radio activity.

Section 2 of this paper describes our galaxy sample. Section 3 presents observations made at the VLA and the reduction of these data. Analyses of the radio and optical properties, including the radio morphology and the radio luminosity function are described in Sec. 4. Section 5 is a discussion of the results of both Paper I and this paper. Discussion of individual clusters is given in the appendix. $H_0=75$ km/s/Mpc and $q_0=0$ have been used throughout both papers.

TABLE 1. z Distribution of observations and detections ($z<0.13$).

z Bin Range	Number of Clust.	Count per Unit Volume	Number of Detect.	Detection Ratio	Poisson Error	BV Detct. Ratio
0.02-0.039	9	59.9	5	0.56	0.25	0.71
0.04-0.059	16	39.3	4	0.25	0.13	0.33
0.06-0.079	26	32.8	10	0.38	0.12	0.27
0.08-0.099	17	13.0	5	0.29	0.13	–
0.10-0.119	11	5.64	4	0.36	0.18	–
0.12-0.13	12	7.17	2	0.17	0.12	–

2. THE SAMPLE

The Abell clusters observed by the VLA were selected from Struble & Rood's (1987) catalog of the morphological properties of 2712 clusters. In addition, the Parkes source PKS 0745−191 was included. Redshifts were taken from Struble & Rood (1982, 1991).

Our final observed sample included 88% of the Abell clusters out to $z<0.10$ that were classified as cD clusters in Struble and Rood's catalog. Struble and Rood identified 76 clusters classified as cDs to that z while our sample included 67 of those clusters. Out to $z<0.133$, our VLA sample includes 80% of the cDs in Struble and Rood's catalog. With 24 hours of VLA observing time allocated to this project, clusters were assigned observing priority according to their distance. Most of the nearby clusters in Struble and Rood's catalog were observed.

Table 1 presents a summary of the distribution of z in the sample. The data were binned in z ranges as indicated in the first column. Column 2 lists the number of observed cDs in each bin. Column 3 is the number of cDs observed per ($\times 10^{-8}$ Mpc^3). Column 4 is the number of radio detections in each z bin. Column 5 is the detection ratio (fraction of observations in our sample that are classified as detections) for each z bin and column 6 is the associated Poisson error for that detection ratio. Four subsamples will be used in this paper: our 6 cm VLA sample with $z<0.1$, our 6 cm VLA sample with $z<0.13$, a 20 cm sample from the Westerbork Synthesis Radio Telescope (Bijleveld & Valentijn 1983) (referred to as BV) that overlaps our sample, and a 20 cm sample from the 91 m Green Bank radio telescope (Owen *et al.* 1982) that also overlaps our sample. Column 7 of Table 1 is the detection ratio of the 20 cm sample from BV.

Overall detection percentages for these samples are: (1) our sample to $z<0.1$, 24 detections from 68 observations or $35\%\pm7\%$; (2) our sample to $z<0.13$, 30 detections from 91 observations or $33\%\pm6\%$; (3) BV, 12 detections from 28 observations or $43\%\pm12\%$; and (4) Owen *et al.* (1982), 35 detections from 85 observations or $41\%\pm7\%$. Given the expected (Poisson) errors associated with each sample, these detection percentages are consistent with each other. Paper I (Burns 1990) reported a subsample size of 27 clusters with *Einstein* x-ray images and 13 radio detections (with many at low z), for a detection percentage of $48\%\pm13\%$.

3. VLA OBSERVATIONS AND DATA REDUCTIONS

The observations were made on 7 and 15 September 1986, by the VLA in the B configuration at 6 cm with a

bandwidth of 50 MHz. Integration time on each source was approximately 5–15 min. As indicated in Table 1, our sample contains a bias toward nearer clusters. The detection ratio for the nearest z bin is significantly higher than any other bin. An attempt was made to reduce this effect during the observing runs by increasing the integration time on each cluster linearly with increasing z. However, limited observing time at the VLA would not allow a complete correction (proportional to z^2).

This VLA configuration resulted in an angular resolution of 1–2 arcsec which allows us to resolve many of the compact sources reported in the 20 cm survey of Zhao *et al.* (1989). Yet, the observations should have reasonable sensitivity to low surface-brightness structures up to about 1 arcmin in diameter. This meant, in some cases, we would not be able to sample all the spatial frequencies associated with larger sources.

The data were calibrated using 3C286 as the primary flux calibrator on the Baars *et al.* (1977) scale. Cleaned maps were produced using the MX program within the NRAO AIPS software package. See Paper I for further details. RMS noise on the final maps of 0.2 mJy per beam was typical. In the processing of some maps, a "natural weighting" was used to emphasize the more heavily sampled inner portion of the u–v plane at the expense of the longer spacings. This was done to better map the extended features of those sources. In some maps, the u–v amplitudes were tapered to improve the detection of any extended structures.

Detection of a cD was claimed if the 6 cm flux density was >3 times the background noise. If no source was discernable near the cD, three times the rms noise level per beam was reported as an upper limit to the flux density.

Table 2 lists the measured optical centroid positions of the cD galaxies in our sample. These measurements were made with the NRAO Mann measuring engine at the VLA and are accurate to about 1″. These positions correspond to the VLA phase centers on each image.

Table 3 presents a summary of all 91 clusters included in this project. The first column identifies the cluster. Column 2 is Abell's count of the number of galaxies within one Abell radius of the center of the indicated cluster. Galaxies included in that count are brighter than two magnitudes fainter than the third brightest member of the cluster (Struble & Rood 1987). Column 3 is the cluster redshift as reported in Struble & Rood (1991). An asterisk following the redshift indicates that value was estimated from the tenth brightest galaxy magnitude, following Batuski & Burns (1985). Column 4 is a description of the radio source structure as further explained in Sec. *4.4*.

Column 5 identifies the source of the 6 cm flux density used to compute the radio power. Our VLA observations of the sources in this study were compared to observations reported in the literature. In several instances (see Appendix), we felt the reported flux densities were more reliable than our VLA data, because of missing short spacings. Based on estimates from 20 cm data, we could be missing flux density from amorphous or other extended sources. But, we were also concerned about background contami-

TABLE 2. Optical centroid positions ($z<0.13$).

Abell Num.	RA H M S	DEC D M S
77	00 37 48.2	+29 16 53
85	00 39 18.7	−09 34 41
126	00 57 24.3	−14 30 50
133	01 00 15.4	−22 09 19
150	01 06 38.9	+12 54 24
151	01 06 22.5	−15 40 24
193	01 22 29.3	+08 26 27
208	01 28 59.1	+00 17 54
267	01 50 41.1	+00 47 35
399	02 55 08.7	+12 49 49
401	02 56 12	+13 23 03
415	03 04 32.7	−12 10 29
496	04 31 20	−13 22 00
505	04 51 51.2	+79 51 51
536	05 05 21.4	−09 19 19
PKS 0745-191	07 45 19	−19 10 10
635	08 08 17.5	+16 15 59
644	08 14 59.2	−07 21 23
690	08 36 13.3	+29 01 15
727	08 55 32.2	+39 04 22
754	09 06 06.3	−09 25 37
763	09 09 48.5	+16 12 22
779	09 16 44	+33 57 29
912	09 58 35.9	+00 09 39
978	10 17 56.2	−06 16 30
1068	10 37 51.5	+40 12 51
1227	11 18 49.1	+48 19 20
1235	11 20 38.1	+19 52 19
1302	11 30 22.1	+66 39 20
1329	11 35 38.1	+71 23 54
1382	11 45 18.3	+71 41 02
1521	12 16 35.1	−13 27 35
1650	12 56 07.3	−01 29 31
1651	12 56 47.5	−03 55 51
1654	12 56 56.0	+30 17 39
1663	13 00 18.2	−02 14 54
1668	13 01 19.2	+19 32 21
1680	13 04 28.6	+40 03 49
1691	13 08 52	+39 29 28
1749	13 27 06.7	+37 52 51
1767	13 34 20.3	+59 27 38
1795	13 46 34.2	+26 50 25
1800	13 47 06.3	+28 21 16
1809	13 50 35.5	+05 23 44
1837	13 58 56.1	−10 53 18
1864	14 05 34.9	+05 39 16
1873	14 09 34	+28 13 02
1890	14 15 09.5	+08 24 36
1924	14 28 39.5	−02 08 51
1927	14 28 52.4	+25 51 10
1982	14 49 07.5	+30 53 54
2029	15 08 27.4	+05 55 58
2052	15 14 17	+07 12 18
2063	15 20 39	+08 47 10
2067	15 21 05.6	+31 03 14
2079	15 25 39.9	+29 05 26
2083	15 27 42.5	+30 52 40
2089	15 30 45	+28 12 23
2107	15 37 27.4	+21 56 34
2110	15 37 49.6	+30 52 42
2124	15 43 05.7	+36 15 53
2128	15 46 06.8	−02 50 29
2170	16 14 51.9	+23 18 30
2175	16 18 32.3	+30 00 32
2199	16 26 55	+39 39 40
2228	16 45 46.9	+30 01 45
2244	17 00 51.9	+34 07 59
2271	17 20 54.1	+78 04 00
2319	19 19 36.7	+43 50 60
2345	21 24 31.2	−12 23 02
2362	21 37 31.2	−14 27 33
2372	21 42 28.1	−20 13 31
2400	21 55 01.8	−11 39 01
2420	22 07 38	−12 25 03
2480	22 43 18.4	−17 53 22
2559	23 10 25.6	−13 53 46
2589	23 21 27.2	+16 30 06
2593	23 21 49.3	+14 22 20
2597	23 22 43.7	−12 23 56
2622	23 32 31.6	+27 05 45
2626	23 33 59.5	+20 52 08
2634	23 35 48	+26 45
2660	23 42 40	−26 06 47
2665	23 48 17.4	+05 52 16
2666	23 48 26.2	+26 52 09
2670	23 51 39.6	−10 41 52
2675	23 53 09.5	+11 03 47
2694	23 59 50.4	+08 07 11
2696	00 00 06.2	+00 39 47
2698	00 00 44.4	+04 20 56
2700	00 01 15.9	+01 47 17

TABLE 3. cD sample ($z < 0.13$).

Abell Num.	Na	z	Radio Source Info	Ref	6-cm Flux Den. (mJy)	P(6) (W/Hz)	B-M Type	Sub-Sample OWHH	Sub-Sample BV	Sub-Sample BBL
77	50	0.0719	Compact	1	4.7±0.3	22.68	I	u		d
85	59	0.0556	Amorphous	3	64.3	23.61	I	d	d	d
126	51	0.1032*	Compact	1	17.6±0.6	23.58	I-II	u		d
133	47	0.0604	Amorphous	3	6.01	22.64			d	d
150	55	0.0596	None	2	<0.72	<21.70	I-II	u		u
151	72	0.0532	None	2	<0.68	<21.57	II	u	u	u
193	58	0.0482	Compact	1	2.1±0.2	21.98	II	u		d
208	41	0.1032*	Double	5	230.0	24.71		u		d
267	37	0.1032*	None	2	<0.63	<22.13		u		u
399	57	0.0715	None	2	<0.42	<21.63	I-II	d	u	u
401	90	0.0748	None	6	<0.24	<21.41	I	d	u	u
415	67	0.0788	None	2	<0.26	<21.50	II	d		u
496	50	0.0327	Compact	1	52.6±1.6	23.03	I	d	d	d
505	39	0.0543	None	2	<0.65	<21.57	I	u	u	u
536	97	0.0398	None	2	<0.93	<21.46	III	u		u
PKS 745-191		0.1028	Amorphous	1	391±12	24.96				d
635	35	0.1309*	None	2	<0.63	<22.34	III	u		u
644	42	0.0704	None	2	<0.63	<21.79	III	u	u	u
690	52	0.0788	WAT	5	399.0	24.69	I	d		d
727	65	0.1096*	None	2	<0.36	<21.94	III	u		u
754	92	0.0544	None	2	<0.30	<21.24	I-II	d	u	u
763	50	0.0971*	Double	5	89.0	24.23	II-III	d		d
779	32	0.0230	None	2	<0.66	<20.83	I-II	d	d	u
912	36	0.0888	None	2	<0.66	<22.02		u		u
978	55	0.0527	None	2	<0.71	<21.58	II	u	u	u
1068	71	0.1309*	Compact	1	1.6±0.2	22.75	I	u		d
1227	112	0.1120	None	2	<0.60	<22.18	II-III	u		u
1235	122	0.1042	None	2	<0.56	<22.09	II	u		u
1302	85	0.1168	None	2	<0.63	<22.24	II	u		u
1329	59	0.0971*	None	2	<0.21	<21.60	I-II	d		u
1382	57	0.1053	None	2	<0.39	<21.94	II	u		u
1521	65	0.0937	None	2	<0.60	<22.02	III	u		u
1650	114	0.0845	None	2	<0.93	<22.12	I-II	d		u
1651	70	0.0845	None	2	<0.78	<22.05	I-II	u		u
1654	31	0.1234*	None	2	<1.05	<22.51	I	u		u
1663	56	0.1309*	None	2	<0.72	<22.40	II	u		u
1668	54	0.0649	Core/Jet	1	>12.4±0.4	>23.01	II	u		l
1680	47	0.1309*	None	2	<0.69	<22.38				u
1691	64	0.0722	None	2	<0.57	<21.77	II	u	u	u
1749	55	0.0590	None	2	<0.72	<21.69	II	u		u
1767	65	0.0701	None	2	<0.66	<21.81	II	d		u
1795	115	0.0621	Double	5	260.0	24.31	I	d	d	d
1800	40	0.0755	None	2	<0.54	<21.79	II	d	u	u
1809	78	0.0789	None	2	<0.86	<22.02	II	u		u
1837	50	0.0376	None	2	<0.54	<21.17	I-II	u		u
1864	77	0.1309*	None	2	<0.54	<22.28	II	u		u
1873	41	0.0776	None	2	<0.54	<21.81	II	u		u
1890	37	0.0570	None	2	<0.79	<21.70	I-II	d	u	u
1924	95	0.1309*	None	2	<0.41	<22.16				u
1927	50	0.0740	None	2	<0.23	<21.39	I-II	d		u
1982	49	0.1032*	None	2	<0.52	<22.05	I-II	u		u
2029	82	0.0768	Double	3	100.0	24.09	I	d	d	d
2052	41	0.0348	Amorphous	5	1038	24.40	I-II	d	d	d
2063	63	0.0355	Double	1	7.7±0.4	22.30	II	u	u	d
2067	58	0.0748	None	2	<0.54	<21.78	II	u		u
2079	57	0.0656	Double	5	112.0	23.99	II-III	d	u	d
2083	60	0.1143	Compact	1	>6.5±0.2	>23.23	III	d		l
2089	70	0.0733	None	2	<0.76	<21.91	II	d		u
2107	51	0.0421	None	2	<0.71	<21.39	I	d		u
2110	54	0.0980	Compact	1	1.8±0.1	22.53	I-II	u		d
2124	50	0.0654	None	2	<0.51	<21.63	I	u	u	u
2128	39	0.0971*	Compact	1	1.2±0.1	22.34	I-II	u		d
2170	38	0.0672*	None	2	<0.69	<21.79	III	u		u
2175	61	0.0978	None	2	<0.69	<22.12	II	u		u
2199	88	0.0299	Double	3	500.0	23.95	I	d	d	d
2228	55	0.1234*	None	2	<0.57	<22.25	I-II	u		u
2244	89	0.0968	None	2	<0.48	<21.96	I-II	d	d	u
2271	35	0.0568	None	2	<0.55	<21.54	I	u		u
2319	68	0.0564	None	2	<0.68	<21.63	II-III	d	d	u
2345	107	0.1234*	None	2	<0.38	<22.09	III	d		u
2362	69	0.0609	Compact	1	5.9±0.2	22.64	II	u		d
2372	41	0.0971*	None	2	<0.34	<21.81				u
2400	56	0.0881	None	2	<0.69	<22.03	II	u		u
2420	88	0.0838	WAT ?	1	3.9±0.2	22.74	I	u		d
2480	51	0.1234*	Double	1	185±6	24.78	II	d		d
2559	73	0.0796	None	2	<0.42	<21.72	I-II	d		u
2589	40	0.0415	None	2	<0.17	<20.76	I	d	u	u
2593	42	0.0433	None	2	<0.54	<21.30	II	d		u
2597	43	0.0852	Double	1	329±10	24.70	III	d		d
2622	41	0.0621	None	2	<0.69	<21.72	II-III	d		u
2626	47	0.0573	Compact	1	7.6±0.3	22.71	I-II	d	d	d
2634	52	0.0309	WAT	4	2800	24.72	II	d	d	d
2660	45	0.0914*	None	2	<0.54	<21.96				u
2665	34	0.0556	Amorphous ?	1	>3.9±0.2	>22.37		u		l
2666	34	0.0270	None	2	<0.60	<20.93	I	d	u	u
2670	142	0.0761	Compact	1	2.2±0.2	22.41	I-II	u	u	d
2675	60	0.0726	Compact	1	3.2±0.2	22.53	II	u		d
2694	132	0.0958	None	2	<0.68	< 22.09	I	u		u
2696	39	0.1234*	None	2	<0.55	<22.23		u		u
2698	83	0.1309*	None	2	<0.57	<22.30	II	u		u
2700	59	0.0978	None	2	<0.63	<22.08	II	u		u

nation in data from lower resolution observations. Code numbers are used to indicate the data source reported: 1—our VLA observation; 2—a 3× background upper limit from our VLA observation; 3—one of the Andernach series of survey papers (III–VII, see the reference section under Andernach); 4—Kellerman *et al.* (1969); 5—Becker *et al.* (1991); 6—Burns & Ulmer (1980). Column 6 presents either integrated 6 cm flux density (in mJy) for each detected source or an upper or lower limit. If our VLA flux density was reported, the error in that flux density was reported using a quadrature formula combining the rms background noise level and 3% of the measured flux density. Column 7 reports the integrated log $P(6)$ radio power computed from the flux density. A "$>$" preceding the flux and the radio power indicates a lower limit flux density due to suspected missing flux density from the VLA observations. The integrated flux density of a source was determined using one of two techniques for the VLA maps. If the source was significantly extended on the map, the flux density was integrated over all the visible source structure. If the source appeared compact, a two-dimensional Gaussian was fit to the brightness distribution and that distribution was integrated. For more details on individual clusters, see the Appendix.

The Bautz–Morgan (1970) classification of each cluster is given as Roman numerals in column 8. The subsample columns indicate which clusters were observed by other studies and are included in our study. Column 9 (OWHH) indicates sources in our total sample which were also included in Owen *et al.* (1982) from the 91 m Green Bank telescope at 20 cm. The 20 cm flux densities were limited to >0.10 Jy. 1476 clusters were observed, of which 442 were detected. This sample included 85 clusters from our sample with 35 detections. However, one must also be concerned that lower resolution can result in an increase in contamination from background sources. Column 10 (BV) indicates sources also included in Bijleveld & Valentijn (1983). These data were taken with the Westerbork Synthesis Radio Telescope operating at 20 cm and from the literature. The rms noise level was 1.1–1.6 mJy per beam. Of the 66 clusters observed, 28 were included in our sample. Column 11 (BBL) reports our entire VLA sample ($z<0.13$) of 91 sources. In each of the columns 8–10, the following notation has been used: *d* indicates a detection, *u* indicates an upper limit, *l* indicates a lower limit, and a blank indicates that cluster was not included in that sample. Detection ratios for each of these four subsamples was discussed at the end of Sec. 2. Detections and upper limits reported in these columns are as they were indicated in the literature, not based on our definition of a detection.

Great care was exercised in the collection of our sample. Our integrated radio power and 6 cm radio maps were compared to the results of other researchers: principally Andernach; Bijleveld and Valentijn; Owen; O'Dea and Baum; and Becker *et al.* If our 6 cm flux density was in good agreement with other results and our optical positions were within about 10 arcsec of their radio position, we reported our VLA results. In cases where single dish flux density measurements were significantly higher than our results, we assumed that we did not observe all the flux density using the VLA and data from the literature were reported. In cases where the 6, 11, or 20 cm position reported in the literature was significantly different from our optical position or the field was confused by the presence of many other radio sources, our data were reported as either a detection or an upper limit. 11 and 20 cm data were used (when available) to estimate the 6 cm flux density by assuming a spectral index appropriate for that source type (compact, WAT, etc.) Comments on individual clusters in our sample are in the Appendix.

4. COMPARISON OF RADIO AND OPTICAL PROPERTIES

Because it is more complete, our $z<0.1$ sample was used to investigate the relationship between 6 cm radio power and Bautz–Morgan type, cluster richness, cD galaxy ellipticity, and radio morphology. Also, a survival analysis technique was used to develop a radio luminosity function. We now describe the results of these investigations.

4.1 Bautz–Morgan Type

Bautz & Morgan (1970) classified clusters based on the relative contrast of the brightest member in the cluster. B–M type I clusters are dominated by a central large, supergiant galaxy. In B–M type II clusters, the brightest galaxies are intermediate between supergiant and giant ellipticals of the Virgo type. B–M type III clusters have no dominant galaxies. Types I-II and II-III are intermediate classifications. We note that cD galaxies do occur in all Bautz–Morgan classes since cDs have been defined as having an extended amorphous halo surrounding a very luminous central core. Several studies have focused on the radio emission of all galaxies in a cluster, rather than concentrating on just cDs. McHardy (1979) noted that B–M type I clusters appear more radio luminous at 178 MHz than type II or III. Owen (1975) found B–M types I to II-III to be equally likely to have radio emission at 20 cm while B–M type III clusters were somewhat less likely. Zhao *et al.* (1989) investigated the relationship between 20 cm radio emission and B–M type. They failed to detect any significant enhancement of radio-detection rates with B–M type. In this paper, we ask if the degree of optical dominance of the cD galaxy (as given by Bautz–Morgan type) influences the probability of radio emission.

Our $z<0.1$ subsample of 68 sources included 63 with B–M types. Figure 1 indicates a slightly enhanced detection rate and a higher average radio power for cDs in B–M type I clusters. Arrows represent upper and lower limits while ×'s indicate detections. The horizontal scale is as follows: 1/I, 1.5/I-II, 2/II, etc. The majority of the detections are in the lower B–M type section of the graph while the majority of the upper limits fall in the middle range of B–M type. Table 4 provides data and statistics for those clusters having an assigned B–M type. Column 1 indicates B–M type. Column 2 is the number of clusters in our $z<0.1$ sample for each B–M grouping while column 3 is the number of detections or lower limits in that grouping. Column 4 is the detection ratio while columns 5 and 6

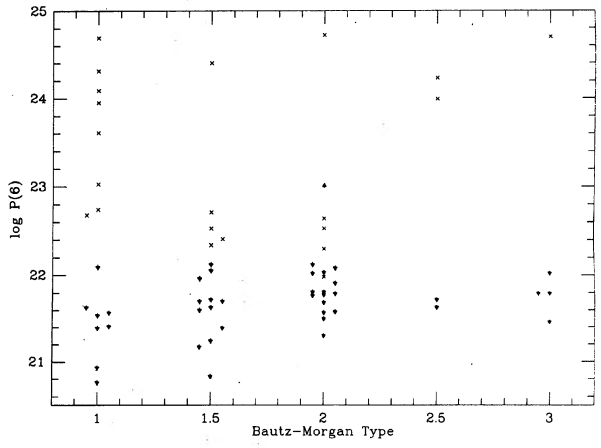

FIG. 1. Bautz–Morgan type vs 6 cm radio power for sources with $z<0.1$. $\times$'s indicate detections, downward arrows indicate upper limits, and upward arrows indicate lower limits. The Bautz–Morgan classification has been converted to Arabic numbers and the plotted values have been spread horizontally.

present the Kaplan–Meier (KM) estimated mean 6 cm radio power and error of estimate for detected and upper limit sources. A more complete discussion of the ASURV statistical package and the Kaplan–Meier estimator can be found in Sec. *4.5*. The last line of Table 4 combines data for all clusters of B–M types greater than I.

The enhanced detection ratio for B–M I clusters could be due to their being at lower average redshift than all other B–M types. In fact, the various two-sample tests in ASURV indicate that the B–M I redshift population is different from all other B–M types at the 90%–95% confidence level. The KM estimate of the average redshift is 0.0593 ± 0.0050 for B–M I's and 0.0686 ± 0.0029 for all other B–M types. However, the enhanced detection rate for B–M I's is still apparent even at high redshift. For example, we detected four out of six B–M I clusters at $z>0.07$, but only five out of 26 clusters having all other B–M types in that same z range. The KM estimates (column 5) indicate that B–M I's have a higher average 6 cm power than the average of all other B–M types. This observation is supported by ASURV two-sample tests which indicate that B–M I and all other B–M type radio power distributions are drawn from different populations to the 90%–95% confidence level.

The radio spectral index between 6 and 20 cm also appears to be related to B–M type. Of the 22 detections in our sample having B–M type, nine were found to also have reliable 20 cm flux densities. Table 5 indicates that clusters with high spectral index (greater than 0.75) are predominantly B–M type I to I-II. The two cDs with lower spectral

TABLE 4. Detection ratio and average 6 cm power ($z<0.1$).

Bautz-Morgan Type	Number of Clusters	Number of Detections	Detection Ratio	K-M Mean P(6)	K-M Error +/-
I	16	8	0.50	22.2	0.4
>I	47	14	0.30	21.5	0.2

TABLE 5. Spectral Index and B-M Type for $z<0.1$ Sample Detections

Abell Num	Radio Source Info	P(6) W/Hz	Computed Spectral Index	BM Class	20 cm Data Source
2079	Double	23.99	0.55	II-III	Zhao,Burns,Owen (1989)
763	Double	24.23	0.58	II-III	Owen, White, Burns (1992)
690	WAT	24.69	0.75	I	Owen, White, Burns (1992)
2634	WAT	24.72	0.80	II	Owen et al. (1982)
1795	Double	24.31	0.82	I	Owen, White, Ge (1993)
2052	Amorphous	24.40	1.31	I-II	Zhao,Burns,Owen (1989)
2029	Double	24.09	1.42	I	Owen et al. (1982)
2199	Double	23.95	1.55	I	Owen et al. (1982)
85	Amorphous	23.61	1.74	I	Owen et al. (1982)
133	Amorphous	22.64	2.82		Slee & Reynolds (1984)

index are of B–M type II-III. Unfortunately, the subsample size is quite small. If steeper spectral index sources are more common in B–M I clusters, this might explain why those clusters are more often detected at 178 MHz (McHardy 1979) than at 1.46 GHz (Owen 1975). When $P(6)$ was compared to spectral index, no significant relationship was apparent.

4.2 Richness

Does the global cluster environment affect the probability of radio emission for a central cD? Richness is a good measure of cluster environment. Richness of the cluster was determined using Abell's counts of the number of galaxies as described above (Struble & Rood 1987). At 20 cm, Zhao *et al.* (1989) found a weak correlation in detection ratio with richness for all radio galaxies in clusters. As cluster richness increased, the percentage of detections increased slightly. Figure 2 plots log $P(6)$ against richness for each cD cluster in the sample. $\times$'s indicate detections while arrows indicate upper or lower limits. The majority of observed clusters had richness between 30 and 80. There does not appear to be any significant dependence of cD radio properties on cluster richness.

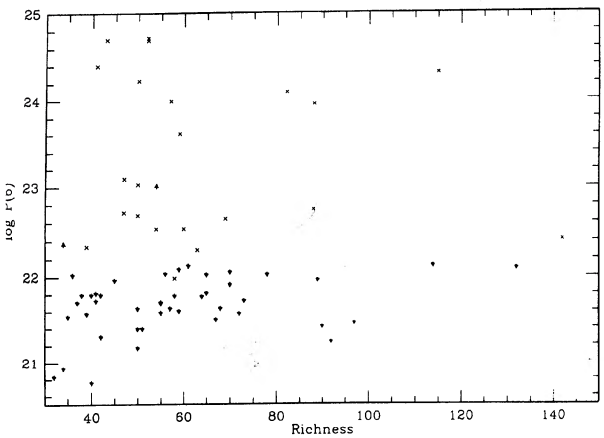

FIG. 2. Richness vs 6 cm radio power for sources with $z<0.1$.

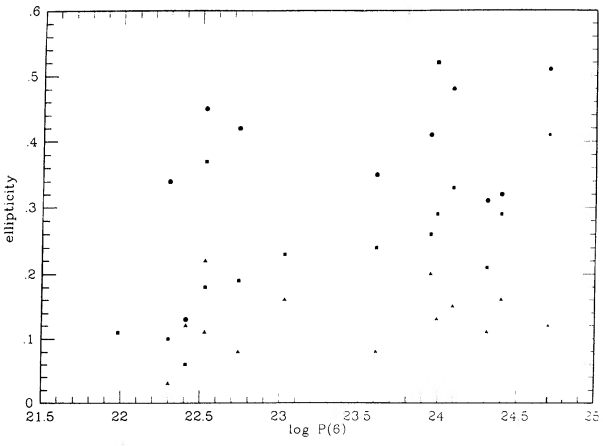

FIG. 3. 6 cm radio power vs optical ellipticity for sources with $z<0.1$. Triangles represent ellipticity values 4 kpc from the optical center, squares represent 16 kpc ellipticity values, and circles represent 64 kpc ellipticity values. All data represent radio detections only.

TABLE 6. Separation and RAM values ($z<0.1$).

Abell Number	Separation Kpc	RAM	log P(6)
85	–	20.78	23.61
126	90.3	–	23.58
193	24.3	20.90	21.98
496	–	21.21	23.03
1068	108.8	–	22.75
1795	–	21.05	24.31
2029	–	20.36	24.09
2052	186.1	21.22	24.40
2063	–	21.31	22.30
2079	712.6	20.83	23.99
2110	340.8	21.02	22.53
2199	–	20.65	23.95
2362	167.4	–	22.64
2420	–	20.89	22.74
2597	–	21.26	24.70
2634	436.7	–	24.72
2670	–	20.75	22.41
2675	–	21.18	22.53

4.3 cD Optical Properties

Do the shape and luminosity of the cD, and the proximity of apparent companion nuclei affect the generation of radio sources in cDs?

Various studies (Disney *et al.* 1984; Sparks *et al.* 1984; Calvani *et al.* 1989) have indicated that radio galaxies, as a class, are significantly rounder than radio-quiet ellipticals. We investigated possible relationships for cDs between $P(6)$ and optical ellipticity (at 4, 16, and 64 kpc from the optical center) using data from Porter *et al.* (1991). This paper is based on a sample of 175 brightest cluster elliptical galaxies observed with the Palomar 1.5 and 5 m and the KPNO 2.1 m telescopes. Porter *et al.* fit the isophotes of their R band CCD images to ellipses at intervals of 0.25 mag. The authors reported that at radii <16 kpc, these galaxies appear rounder than the average elliptical galaxy. However, at radii greater than 30 kpc, they become so highly elliptical that they cannot be represented by a random orientation of oblate spheroids. They searched for a correlation between the ellipticity of the galaxies in their sample and corresponding radio luminosities from Zhao *et al.* (1989) and from Paper I. They were unable to detect a correlation, but the sample size (27 galaxies) was small.

Using their data that overlapped clusters from our $z<0.1$ subsample in which we had detections, we attempted to discover if a relationship exists for cDs between ellipticity at various radii and radio power. Our data contained fourteen clusters with z values from 0.03 to 0.098. Porter *et al.* conducted several experiments to determine the effect of seeing on their estimates of the shape parameters. They concluded that even at the radius of the seeing disk, the ellipticity of a galaxy with a King profile was generally within 0.1 of its true value. We observed no significant differences between average ellipticities at 4, 16, and 64 kpc in Porter *et al.*'s brightest cluster galaxy sample and our cD subsample of their data. For radio loud cDs (detections), Fig. 3 plots ellipticity against log $P(6)$ with triangles indicating 4 kpc ellipticity, squares indicating 16 kpc ellipticity, and circles indicating 64 kpc ellipticity. Linear regressions were performed on these data yielding the following correlation coefficients and probabilities of being significant: $r^2_{4\text{kpc}}=0.044(55\%)$, $r^2_{16\text{kpc}}=0.469(99.3\%)$, and $r^2_{64\text{kpc}}=0.141(73\%)$. While the 4 and 64 kpc data indicate no relationship between $P(6)$ and ellipticity, there appears to be a correlation between the 16 kpc ellipticity and 6 cm radio luminosity.

Next, we investigated a possible relationship between radio and optical luminosities using Hoessel & Schneider's (1985) optical data on 16 kpc aperture magnitudes of the same 175 Abell clusters studied by Porter *et al.* (1991). Table 6 identifies 14 clusters with radio detections from our $z<0.1$ subsample that overlap the Hoessel–Schneider sample. Hoessel and Schneider reported RAM (reduced absolute magnitude) values that represent the K-corrected apparent g magnitude of an object placed at a luminosity distance of one Hubble radius ($H_0=60$ Km/s/Mpc). Linear regression analysis produced an $r^2_{\text{RAM}}=0.0135$, indicating no relationship. However, the range in optical magnitude for our cD sample is small (about 1 mag).

We also investigated the possibility of a relationship between log $P(6)$ and the separation of the cD optical center from a nearby (projected) satellite, as reported in Struble & Rood (1987). Considering studies by Blandford & Icke (1978), Stocke (1978), and Jägers & de Grijp (1985) concerning the influence of a nearby interacting galaxy on the radio structure, we might expect to find a relationship between these optical properties and 6 cm radio power. Furthermore, Parma *et al.* (1991) reported a narrower distribution of radio power in dumbbell galaxies than in nondumbbell galaxies, indicating that the presence of a companion galaxy might have an effect on the radio power. They also found a relationship between the wavelength of oscillations along the radio jets of dumbbell galaxies and the largest linear size (in kpc) of the dumbbell. Thus, one would expect that the closeness of companion nuclei and tidal interactions should have an effect on radio emission of the cD. Unfortunately, only eight detections in our sample

overlapped clusters in Strubble and Rood where separations between a cD and its nearby satellite galaxy were reported (see Table 6). Though the data is very sparse, we attempted to relate this separation (converted to kpc) to $P(6)$ radio power. Linear regression analysis produced a $r^2_{\text{kpc separation}}=0.276$, indicating no relationship. Such a relationship could be hidden by the small numbers or by contamination due to projections of outer galaxies onto the cores of the clusters. Further information on companion separations and the velocities of nearby companions (to eliminate possible interlopers) are needed before any useful conclusions can be drawn.

4.4 Radio Morphology

The data set in Table 3 was separated into the following radio morphological types:

(1) None—no significant radio source was detected.

(2) Compact—the source was unresolved or only marginally resolved.

(3) Core/Jet—a core structure was observed with an associated jet, but little or no additional extended radio structure.

(4) Amorphous—the source consists of a compact central region completely surrounded by a diffuse halo region

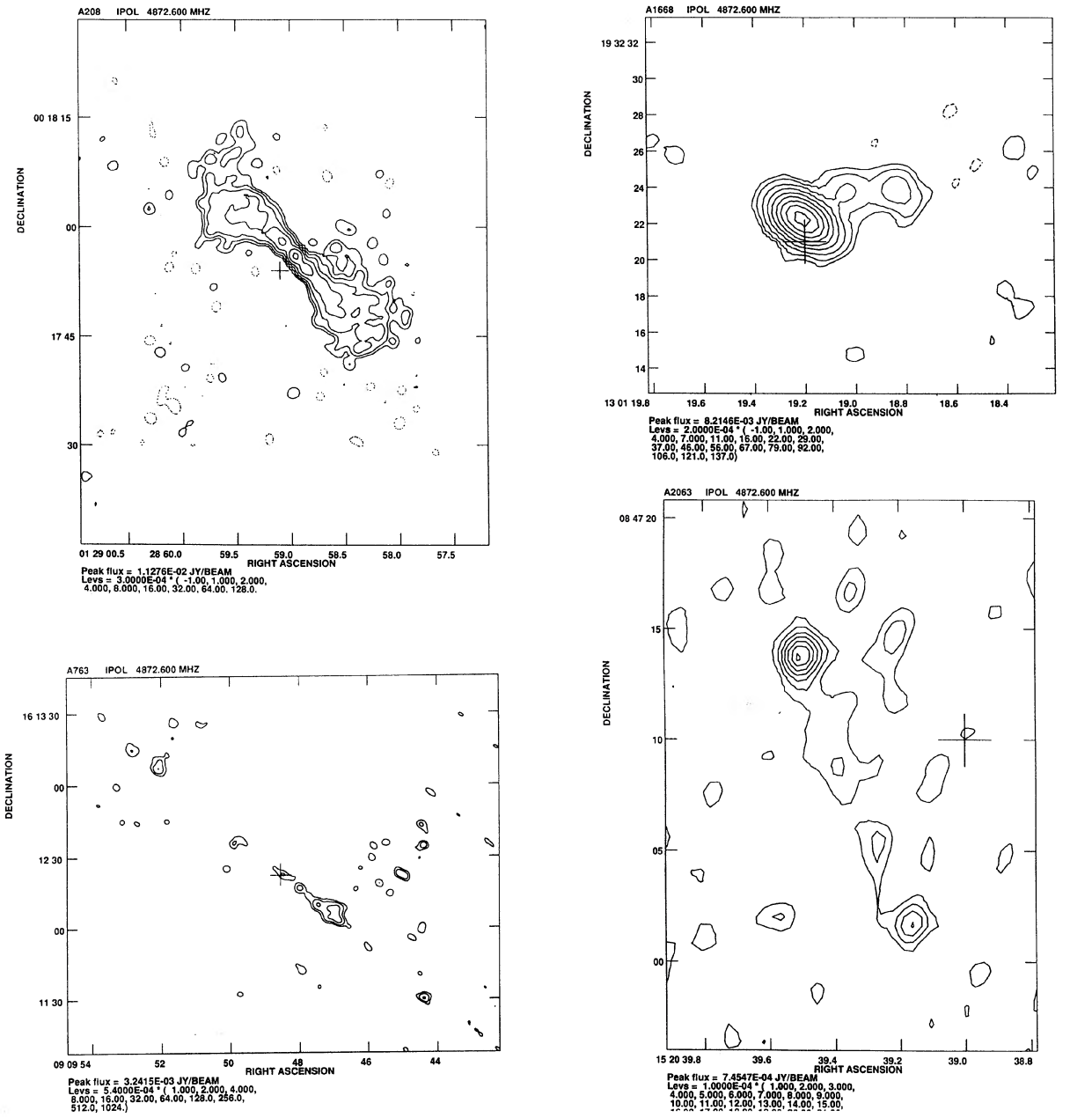

FIG. 4. Contour plots of the new VLA observations of extended sources in this sample. Crosses represent the optical position of the cD as reported in Table 2.

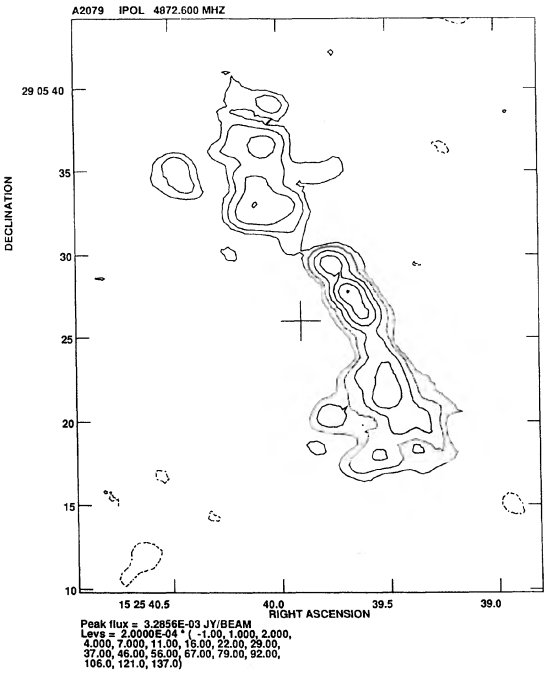

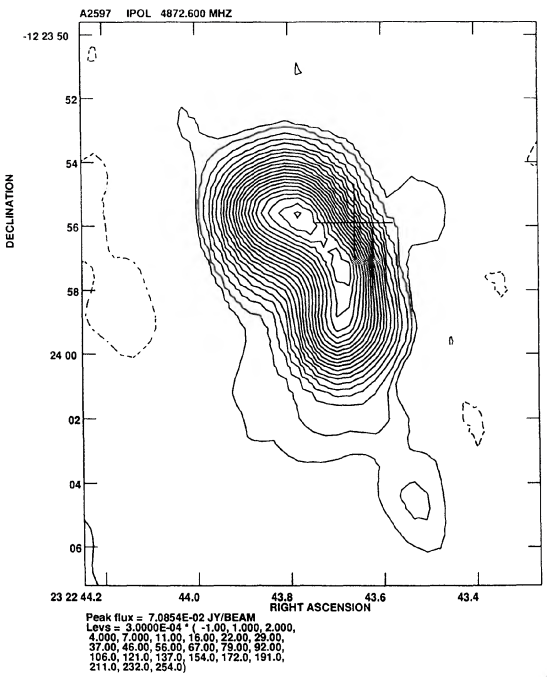

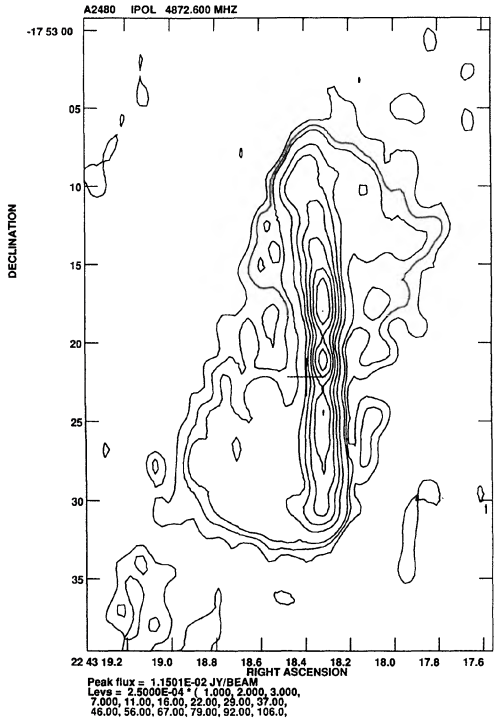

FIG. 4. (continued)

of low surface brightness. The halo usually exhibits a steep spectral index (see Paper I).

(5) Double—radio lobe emission is observed on opposite sides of the core region (usually separated by roughly 180°).

(6) WAT—the source exhibits a wide-angle tailed structure (Rudnick & Owen, 1977).

Figure 4 presents 6 cm radio maps of the following sources and morphological types: double—A208, A763, A2063, A2079, A2480, A2597; core/jet—A1668. Paper I presents 6 cm radio maps of the following sources and morphologies: amorphous—A85, PKS 0745−191, A2052; double—A1795, A2029, A2063, A2199; WAT—A2420, A2634.

A statistical study of the distribution of radio morphologies is presented in Table 7. This table includes all detec-

TABLE 7. Average 6 cm power and average z by morphological type ($z<0.1$).

Radio Morphology	log P(6) Avg	P(6) St. Dev.	z Avg	z St. Dev.	Sources Observed	Percent of Detections
Compact	22.54	0.289	0.0683	0.0214	9	37.5
Core/Jet	23.01	—	0.0649	—	1	4.2
Amorphous	23.27	0.920	0.0516	0.0114	4	16.6
Double	23.94	0.765	0.0646	0.0248	7	29.2
WAT	24.05	1.135	0.0645	0.0292	3	12.5
				Total	24	

tions in our $z>0.1$ sample. The average and standard deviation of the log $P(6)$ power and average z are presented as well as the number of sources assigned that morphological type. Compact sources were definitely the most commonly detected morphology (9 sources out of a total of 24 observations—22 detections and 2 lower limits) but also represent the lowest average power. As Table 7 indicates, double and WAT sources have the highest average power while WAT and amorphous sources display the largest variation in power.

4.5 Radio Luminosity Function

Radio luminosity functions (RLFs) are a useful tool for comparing the distributions of radio luminosities for different types of galaxies in different environments. Due to the difficulty of determining the RLF of a radio galaxy population, many different approaches have been attempted. Our approach will be to use the survival analysis methods of ASURV Rev 1.1 (Isobe & Feigelson 1990), which implements the methods presented in Feigelson & Nelson (1985), to develop a RLF using both measured 6 cm detections and upper limits from our $z<0.1$ subsample. The Kaplan–Meier estimator in the ASURV package was used on our univariant data consisting of 45 upper limits and 22 detections. The ASURV statistical software package was originally developed to apply statistical methods to censored data—data composed of a mixture of measured values and upper or lower limits. Our interest in this software was to produce a RLF from our censored data. In the past, various techniques have been employed to handle data of this type. Some researchers have simply omitted the upper limit values from consideration. Others have divided the data into detected and undetected subsamples. These techniques do not make efficient use of all the available information.

The Kaplan and Meier estimator (KM) used in this analysis produces a maximum-likelihood estimate of the true distribution of a censored input data sample. The log of the fraction of clusters having higher radio power than some value $P_6(\log \mathrm{Fr})$ is computed as log(KM). In Fig. 5, the cD RLF line represents the luminosity function (plotted as log Fr) for the cDs in our $Z<0.1$ subsample. The error bars represent the range of error in the Kaplan–Meier estimator. The jumps in the function are caused by regions of $P(6)$ that have a higher than average concentration of detections.

Our luminosity function indicates that cDs produce 6 cm radio emission at low as well as high power levels. Previous studies (e.g., BV) were insensitive to the lower

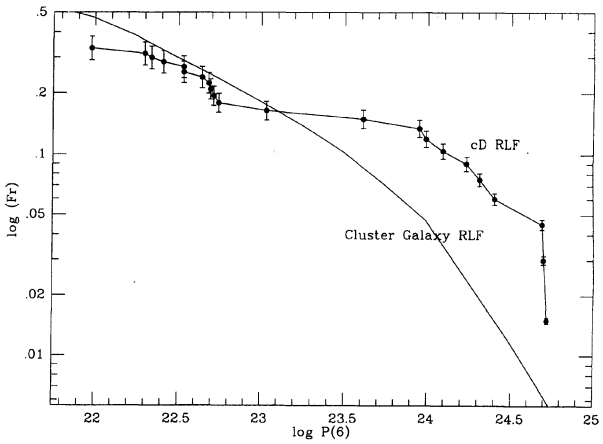

FIG. 5. Integrated radio luminosity functions (RLFs) from our $z<0.1$ sample (plot with circles and error bars computed using the ASURV statistical package) and Fanti's (1984) radio luminosity function (smooth curve).

power levels. Our 6 cm RLF has a lower limit of about 3×10^{21} W/Hz. Note that the grouping of half of the detected sources in our sample around log $P(6)=22.5$ produced a significant rise in our RLF in that region. This could imply that actual cD RLF extends well below our sensitivity level. Low radio power cDs seem to be as probable as high radio power cDs.

Fanti (1984) developed a RLF for all radio galaxies in clusters from high resolution aperture synthesis observations at 20 cm. His RLF represents the number of radio galaxies per average cluster, as a function of radio power at 20 cm. We have adjusted Fanti's RLF (labeled Cluster Galaxy RLF) to representative 6 cm power levels using a spectral index of 0.7, as displayed in Fig. 5. The vertical position of Fanti's RLF was arbitrarily adjusted to overlay our RLF. The knee of both RLFs occur at about 10^{24} W/Hz. However, either our RLF exhibits excessive bright sources (above the knee) or the slope of our RLF below the knee is flatter in comparison to Fanti's RLF, or some combination of both possibilities is involved. The general slope of our RLF above the knee is in good agreement with Fanti's RLF, indicating that the population of bright sources may be similar. Fanti also found that lower B–M type first ranked galaxies (FRG) exhibit a RLF having a visibly flatter slope for lower power sources than FRGs with higher B–M type, in agreement with our Fig. 5. Our sample contains a large percentage of low B–M type sources, implying a possible relationship between low power RLF slope and B–M type. Thus, we see an interesting, and distinctive, difference between the RLFs of cDs and nondominant ellipticals in clusters.

5. DISCUSSION

Several properties of cDs seem to affect the level of radio emission. cD radio emission at 6 cm appears to be strongly influenced by the presence of x-ray cooling cores. Paper I reported that of the cD clusters studied, 71% with cooling cores have central radio emission while only 23% of those

clusters without cooling flows are radio-loud. A possible explanation is that some of the cooling gas reaches the central engine and powers the radio emission. Other ideas presented in Paper I include cosmic ray electron heating of the gas in the cluster center and magnetic field reconnection balanced by radiative cooling. Further study is needed to better understand this connection between cooling cores and radio power.

Also, the presence of cooling cores in cD galaxies may steepen their radio spectrum, indicating that higher central pressures in cooling cores confine the radio-emitting plasma. This confinement should result in greater energy loss through synchrotron emission. The new class of amorphous sources are good examples of this confinement.

Wide angle tailed galaxies (WATs) appear to be a significant class of radio sources that do not exhibit cooling cores. This indicates that mechanisms other than cooling gas inflow can produce relatively powerful, extended radio sources.

B–M type (an indication of the optical dominance of the central galaxy in the cluster) seems to have an effect on both the radio activity and the spectral steepness of cDs. Lower B–M type cDs tend to have a slightly higher detection ratio and a steeper spectral index. Additionally, the B–M type seems to have an effect on the slope of the lower power end of the cD RLF. Lower B–M type sources, as a group, may exhibit a flatter slope in that power range.

Cluster richness (an indicator of the cluster environment) seems to be unrelated to radio activity. The weak correlation between detection ratio and richness reported by Zhao *et al.* (1989) at 20 cm was not observed at 6 cm.

The optical properties of cDs seem to have little influence on the radio properties. No relationship was observed between absolute magnitude, 4 or 64 kpc ellipticity, or separation of nearby companions with radio power. However, a relationship was found between 16 kpc ellipticity and the radio power of detected cDs. An increasing ellipticity correlated with increasing 6 cm radio power, implying that larger distortion (perhaps resulting from a previous merger) produces a slight increase in radio power.

Morphologically compact radio sources exhibit a higher detection ratio that any other morphological type studied for cDs. They also have the lowest average 6 cm power and the highest average z. As expected, double and WAT classifications produced the highest average 6 cm radio power. Observed morphologies do appear to be correlated with radio power.

Our RLF exhibits power on lower levels than either the BV or Fanti (1984) RLFs. However, after spectral index corrections were applied, the position of the knee and the overall shape above the knee are in good agreement. Below the knee, our cD RLF appears flatter than Fanti's RLF. Fanti reports that the RLF of FRGs is flatter with increasing optical dominance (lower B–M type). This would imply a flatter slope for cDs compared to nondominant ellipticals. Our RLF displays this flattening below the knee in comparison to Fanti's RLF. This implies a difference in the two populations, perhaps caused by differences in average B–M type and galaxy formation/evolution.

In conclusion, an x-ray cooling core, indicating the presence of hot gas near the cD core, seems to have the strongest influence on cD radio emission, while global conditions in the cluster do not appear to have a significant effect. Optical properties seem to have only a minor effect, with 16 kpc optical ellipticity being correlated with 6 cm radio loudness. The RLF developed in this study indicates that cDs extend to lower radio power levels than previously seen and the slope of the curve in the low power region may be related to the predominant B–M type.

We would like to thank F. N. Owen for the use of his unpublished 20 cm VLA data and his comments on the text, and J. W. Moody and M. Newberry for their help with the original observations. This work was supported in part by NSF Grant Nos. AST-8611511 and AST-9012353 to J.O.B.

APPENDIX: COMMENTS ON INDIVIDUAL CLUSTERS

A77. We detect a compact source (4.6 mJy) having a $2.28'' \times 1.21''$ angular size and a PA of 108° (from a 2-D Gaussian model fit). No 20 or 11 cm data were found to be associated with this source.

A85. Our data indicate an amorphous source associated with this cD. However, our detection of only 11 mJy seems much too low in comparison with Andernach *et al.*'s (1986) detection of 125 mJy at 11 cm. Using a typical spectral index of 1, we estimate a 6 cm total flux density of 64 mJy from the Andernach *et al.* data. Our missing flux density at 6 cm was probably due to a lack of short baselines in the B configuration. This would cause the VLA to be less sensitive to the extended structure of an amorphous source and more sensitive to any central structure. This recurring problem will be referred to as short baseline flux density loss. The 6 cm maps of this source may be found in Paper I.

A126. We detect a compact source (17.6 mJy). No other report of associated radio emission was found in the literature.

A133. Reuter and Andernach (1990) reported a source labeled #2 in their paper that appears to be associated with the cD. Their 6 cm integrated flux density was less than 15 mJy. Slee & Reynolds (1984) reported a 6 cm power of 22.7 for a steep spectrum amorphous source associated with this cD. This power was reported in Table 3, since we did not detect any source at 6 cm in the VLA's B configuration. See Paper I for a discussion of this source.

A150 and A151. No 6 cm radio sources were detected and no associated detections were found in the literature. We report these sources as upper limits.

A193. Our data indicate a 2 mJy source about 15 kpc from the cD's optical centroid (corresponding to 15″). Due to the large size of this cD, we assumed this radio source to be associated with the cD.

A208. Becker *et al.* (1991) reported a source of 6 cm flux density of 230 mJy which we associate with the cD, given the positional agreement. Our detection of 187 mJy is in good agreement with the Becker *et al.* flux density. The

Parkes catalog also reports a 6 cm flux density of 230 mJy. Becker *et al.*'s single dish flux density was reported in our Table 3.

A267. Our survey failed to detect any 6 cm emission from this cluster and a literature search failed to discover a report of associated radio emission.

A399. Our data indicate a possible very weak, compact radio source associated with the cD. We used three times our VLA rms noise level as an upper limit in our table.

A415. Our data indicate a nonassociated 6 cm source in this field. Owen *et al.* (1982) detected a 20 cm source 6′ from the optical centroid of this cluster. We report this cD as a nondetection and assign an upper limit of three times our VLA rms noise level.

A496. We detect a compact source (52.6 mJy) having a deconvolved size of $0.37'' \times 0.15''$ and a PA of 170°. Andernach *et al.* (1988) reported very complex 6 and 11 cm maps for this region. The cD's optical position appears associated with their source #1 (6 cm integrated flux density of 68 mJy). We report our data for the compact structure associated with this cluster in Table 3. See Paper I for a discussion of this source.

PKS 0745-191. We detect a 6 cm flux density of 390 mJy for this Parkes radio source. This is in close agreement with the 410 mJy integrated flux density reported in the Parkes catalog. The angular size of this source is about $10'' \times 9.6''$. The 6 cm maps of this source may be found in Paper I and also in Baum & O'Dea (1991).

A690. Becker *et al.* (1991) detected a 399 mJy 6 cm radio source which we associate with the cD. Our data indicate a 6 cm flux density of 143 mJy. Our lower flux density was due to short baseline flux loss. Becker *et al.*'s single dish flux density is included in our Table 3. Owen *et al.* (1992) reported a 20 cm flux density of 1022 mJy. See O'Donoghue *et al.* (1990) for a discussion and maps of this WAT.

A754. Andernach *et al.* (1988) maps indicate that this cD is between two large and possibly unassociated radio sources. We saw no associated radio emission on our VLA maps and therefore used three times our VLA rms noise as an upper flux density limit in Table 3.

A763. Our detection of 21.6 mJy is probably too low due to missing short spacings, making it difficult to properly define the morphology of this extended source. Becker *et al.* (1991) reported a 6 cm flux density of 89 mJy associated with the cD, which we use in Table 3. Owen *et al.* (1982) reported an integrated 20 cm flux of 150 mJy. Our map (see Fig. 6) indicates a large jet structure centered on the optical centroid of the cD.

A779. This cluster presents a very confused field. Andernach *et al.* (1981) reported 11 cm maps that show six sources within 4′ of the optical center of this cD. We were not able to identify 6 cm radio emission associated with the cD's optical centroid. Thus, we quote an upper limit in Table 3.

A1068. We detect a compact source (1.6 mJy) centered on the cD's optical centroid position. No other radio detections were found in the literature.

A1668. Our map indicates a double structure with a 6 cm flux density of 12.4 mJy. Owen *et al.* (1993) found a 20 cm source associated with the cD having a 64.7 mJy flux density. This indicates a spectral index of 1.2. Thus, we reported our 6 cm flux density as a lower limit. Our map indicates an angular size of $10'' \times 6''$.

A1749. Owen *et al.* (1993) reported a 20 cm VLA flux density of 12 mJy associated with the cD. Using Owen *et al.*'s flux density and a 0.7 spectral index, the 6 cm flux should be about 5 mJy. However, our data do not reveal a source associated with the cD. Therefore, either our observation resolved a possibly amorphous source away (unlikely given Owen *et al.*'s estimate of the size) or this source has a spectral index greater than 2.1.

A1795. (4C 42.26) Becker *et al.* (1991) listed a 6 cm source with a flux density of 260 mJy which we associate with the cD. This agrees with our measurement of 216 mJy. Owen *et al.*'s (1993) 20 cm VLA data indicate a flux density of 724 mJy. This double source appears on our map with an angular size of $14'' \times 15''$. These data imply a spectral index of 0.85. See Paper I for a discussion and map of this source.

A1890. Though BV, Andernach *et al.* (1980), and Owen *et al.* (1982) reported radio sources in this area, the positions of their detections do not allow us to associate the reported emission with the cD. Our observations did not detect a 6 cm source identified with the cD.

A2029. Andernach *et al.* (1980) identified a 6 cm source (labeled #2 on his map) that appears to be associated with the cD. He reported a flux density of 100 mJy for this source. Our integrated flux density of 39.4 mJy indicates that we are missing considerable 6 cm emission. Owen *et al.* (1992) reported a 20 cm flux density of 489 mJy associated with this double source. Andernach *et al.*'s flux density is reported in our Table 3. These data imply a spectral index of 1.6. Paper I presents a 6 cm map of this source.

A2052. (3C 317) Becker *et al.* (1991) reported a 6 cm flux density of 1.038 Jy associated with the cD. Owen *et al.* (1982) reported a 20 cm flux density of 5.39 Jy. Zhao *et al.* (1989) and O'Dea & Baum (1986) reported similar 20 cm flux density levels. Our VLA observation produced a 6 cm flux density of 919 mJy. We reported Becker *et al.*'s flux density in our Table 3. These data imply a spectral index of 1.37. See Paper I for a 6 cm map of this source.

A2063. Bijleveld & Valentijn (1983) reported a 20 cm source associated with the cD with a flux density < 85 mJy. O'Dea & Baum (1986) reported a 20 cm flux density of 12.4 mJy for a 9 kpc linear source. We measure a 6 cm associated flux density of 7.7 mJy. Paper I presents a 6 cm map of this source.

A2079. Becker *et al.* (1991) listed a 6 cm flux density of 112 mJy which we associate with the cD. Owen *et al.* (1982) reported an associated 20 cm flux density of 360 mJy. Our VLA measurement is 39.4 mJy, implying considerable missing flux density. Thus, we included the Becker *et al.* measurement in Table 3.

A2083. Our map reveals a 6 cm source with a flux density of 6.5 mJy. Owen *et al.* (1982) reported a 20 cm source possibly associated with the cD having a flux den-

sity of 360 mJy. Using a spectral index of 1.5, this would imply a 59 mJy 6 cm source. This indicates our observation may be missing flux. Thus, we used our data as a lower limit.

A2089. Our data indicate no 6 cm detection of the cD. Owen *et al.* (1982) reported a 360 mJy 20 cm unresolved source possibly associated with the cD. If Owen *et al.*'s source is associated, then it must have a very steep spectral index or we have resolved it out. We report no detection for this cD and use three times the background VLA rms noise level as an upper limit.

A2110. We detect a 1.8 mJy compact source having an angular size of $1.3'' \times 0.44''$ with a PA of 28.4°.

A2128. We detect a 1.2 mJy source having an angular size of $0.69'' \times 0.69''$ with a PA of 180°.

A2199. (3C 338) Andernach *et al.* (1980) reported 500 mJy at 6 cm for this source. This flux density agrees with the 6 cm Becker *et al.* (1991) flux density of 477 mJy. Owen *et al.* (1982) reported a 20 cm flux density of 3.48 Jy associated with the cD. This agrees with the BV's (1983) 20 cm flux density of 3.24 Jy. These data imply a spectral index of about 1.6. See Paper I for a 6 cm map of this source. Roland *et al.* (1990) also report observations made with the Westerbork Synthesis Radio Telescope (WSRT) at 608 MHz. See Paper I for a discussion and map of this source.

A2319. Several 6, 11, and 20 cm sources (Andernach *et al.* 1980; Andernach *et al.* 1986; Owen *et al.* 1982; Zhao *et al.* 1989; Baum & O'Dea 1991; Owen *et al.* 1993) were reported in the literature for this area. However, none could be associated with the cD in this confused field.

A2362. We detect a 5.9 mJy compact source having a deconvolved angular size of $0.45'' \times 0.22''$, PA = 81°.

A2420. Our 6 cm data indicate a 3.9 mJy source associated with the cD. Owen *et al.* (1993) measured 12.8 mJy at 20 cm for this source. See Paper I for a 6 cm map of this source.

A2480. Our data indicate a 185 mJy integrated flux density associated with a double structure (angular size: $4.17'' \times 0.65''$). Owen *et al.*'s (1982) 91 m telescope data indicated a 550 mJy source at 20 cm associated with the cD. Owen *et al.* (1992) reported a 364 mJy 20 cm source associated with the cD, as mapped by the VLA.

A2597. Our data reveal a 329 mJy 6 cm source centered on the cD (angular size: $4.63'' \times 1.62''$). Owen *et al.* (1992) report an associated 20 cm source of about 1.7 Jy. This implies a spectral index of about 1.3.

A2622. Our data revealed no 6 cm sources, but Owen *et al.*'s (1993) 20 cm VLA data indicated a slightly resolved amorphous source. We either resolved the image out or this source has a very steep spectral index (3.3).

A2626. (4C 20.57) Our data indicate a compact 7.6 mJy source (angular size: $4.25'' \times 3.46''$, PA: 1.5°) associated with the cD. O'Dea & Baum (1986) reported a 38.5 mJy 20 cm associated source. These data imply a rather steep spectral index (1.3). See Paper I for a discussion of this source.

A2634. (3C 465) Our table reports Kellermann *et al.*'s (1969) 6 cm flux density of 2.8 Jy associated with the cD. Owen *et al.* (1982) reported a 20 cm 7.65 Jy flux density associated with this source. Andernach *et al.* (1988) reported a 2.8 cm flux density of 1.2 Jy associated with this source. These data imply a spectral index of about 0.9. See Eilek *et al.* (1984) for 6 cm VLA maps of this source. Eilek *et al.*'s map and a short discussion of this source are also included in Paper I.

A2665. Owen *et al.*'s (1993) 20 cm VLA data indicated a slightly resolved ($9.7'' \times 3.6''$, PA:23.7°) source with 41.4 mJy integrated flux density identified with the cD. However, our data revealed only a compact source ($0.98'' \times 0.78''$) having a flux density of 3.9 mJy. This could indicate a steep-spectrum amorphous source. Our 6 cm flux density was included in Table 3 as a lower limit.

A2670. Our data indicate a 2.2 mJy compact source about 16 kpc (9″) from the cD. We suggest that this source is associated with the cD.

A2675. Our data indicate a 3.2 mJy compact source about 13 kpc (8″) from the cD. We believe this source is associated with the cD. Owen *et al.* (1993) identified a 20 cm source associated with the cD having a 8.4 mJy flux density. This implies a 0.8 spectral index.

REFERENCES

Andernach, H., Schallwich, D., Haslam, C. G. T., & Wielebinski, R. 1981, A&AS, 43, 155 (Andernach IV)

Andernach, H., Sievers, A., Kus, A., & Schnaubelt, J. 1986, A&AS, 65, 561 (Andernach V)

Andernach, H., Tie, H., Sievers, A., Reuter, H.-P., Junkes, N., & Wielebinski, R. 1988, A&AS, 73, 265 (Andernach VI)

Andernach, H., Waldthausen, H., & Wielebinski, R. 1980, A&AS, 41, 339 (Andernach III)

Auriemma, C., Perola, G. C., Ekers, R., Fanti, R., Lari, C., Jaffe, W. J., & Ulrich, M. -H. 1977, A&A, 57, 41

Baars, J. W. M., Genzel, R., Pauling-Toth, I. I. K., & Witzel, A. 1977, A&A, 61, 99

Batuski, D. J., & Burns, J. O. 1985, AJ, 90, 1413

Baum, S., & O'Dea, C. P. 1991, MNRAS, 250, 737

Bautz, L., & Morgan, W. 1970, ApJL, 162, L149

Becker, R., White, R., & Edwards, A. 1991, ApJS 75, 1

Bijleveld, W., & Valentijn, E. A. 1983, A&A, 125, 223

Blandford, R. D., & Icke, V. 1978, MNRAS, 185, 527

Burns, J. O. 1990, AJ, 99, 14 (Paper I)

Burns, J. O., White, R. A., & Hough, D. H. 1981, AJ, 86, 1

Burns, J. O., & Ulmer, M. P. 1980, AJ, 85, 773

Calvani, M., Fasano, G., & Franceschini, A. 1989, AJ, 97, 1319

Disney, M. J., Sparks, W. B., & Wall, J. V. 1984, MNRAS, 206, 899

Dressler, A. 1978a, ApJ, 222, 23

Dressler, A. 1978b, ApJ, 226, 55

Dressler, A. 1979, ApJ, 231, 659

Edge, A. C., & Stewart, G. C. 1991, MNRAS, 252, 414

Eilek, J. A., Burns, J. O., O'Dea, C. P., & Owen, F. A. 1984, ApJ, 278, 37

Fabian, A. C., Nulsen, P. E. J., & Canizares, C. R. 1991, A&A, Review 2, 191

Fanti, R. 1984, Proceedings of the International Meeting on Clusters and Groups of Galaxies (Trieste), edited by F. Mardirossian, G. Giuricin, and M. Mezzetti (Reidel, Dordrecht), p. 185

Feigelson, E. D., & Nelson, P. I. 1985, ApJ, 293, 192

Gallagher, J., & Ostriker, J. 1972, ApJ, 77, 288
Gunn, J., & Tinsley, B. 1976, ApJ, 210, 1
Hausman, M., & Ostriker, J. 1978, ApJ, 224, 320
Hoessel, J. 1980, ApJ, 241, 493
Hossel, J. G., & Schneider, D. P. 1985, AJ, 90, 1648
Isobe, T., & Feigelson, E. D. 1990, Bull. Amer. Astro. Society, 22, 917
Jägers, W. J., & de Grijp, M. H. K. 1985, A&A, 143, 176
Jones, C., & Forman, W. 1984, ApJ, 276, 38
Kellermann, K. I., Pauling-Toth, I. I. K., & Williams, P. J. S. 1969, ApJ, 157, 1
Mathews, T., Morgan, W., & Schmidt, M. 1964, ApJ, 140, 35
McHardy, I. M. 1979, MNRAS, 188, 495
Merritt, D. 1983, ApJ, 264, 24
Merritt, D. 1984a, ApJ, 276, 26
Merritt, D. 1984b, ApJL, 280, L5
Merritt, D. 1985, ApJ, 289, 18
O'Dea, C. P., & Baum, S. 1986, in Radio Continuum Processes in Clusters of Galaxies, edited by C. O'Dea and J. Uson (NRAO, GreenBank), p. 141
O'Donoghue, A. A., Owen, F. N., & Eilek, A. J. 1990, ApJS, 72, 75
Ostriker, J. P., & Tremaine, S. D. 1975, ApJL, 202, L113
Owen, F. N. 1975, ApJ, 195, 593
Owen, F. N., White, R. A., & Ge, 1993, in preparation
Owen, F. N., White, R. A., & Burns, J. O. 1992, ApJS, 80, 501
Owen, F. N., White, R. A., Hilldrup, K. C., & Hanisch, R. J. 1982, AJ, 87, 1983
Parma, P., Cameron, R. A., & de Ruiter, H. R. 1991, AJ, 102, 1960
Porter, A. C., Schneider, D. R., & Hoessel, J. G. 1991, AJ, 100, 1561
Reuter, H.-P., & Andernach, H. 1990, A&AS, 82, 279 (Andernach VII)
Richstone, D. O. 1975, ApJ, 200, 535
Richstone, D. O. 1976, ApJ, 204, 642
Roland, J., Hanisch, R. J., & Pelletier, G. 1990, A&A, 231, 327
Rudnick, L., & Owen, F. N. 1977, AJ, 82, 1
Sandage, A. 1976, ApJ, 205, 6
Sarazin, C. L. 1988, in X-ray Emissions from Clusters of Galaxies (Cambridge University Press), p. 38
Slee, O. B., & Reynolds, J. E. 1984, Proc. ASA, 5, 516
Sparks, W. B., Disney, M. J., Wall, J. V., & Rodgers, A. W. 1984, MNRAS, 207, 445
Stocke, J. T. 1978, AJ, 83, 348
Struble, M. F., & Rood, H. J. 1982, AJ, 87, 1
Struble, M. F., & Rood, H. J. 1987, ApJS, 63, 555
Struble, M. F., & Rood, H. J. 1991, preprint
Tonry, J. L. 1985, AJ, 90, 2431
Tremaine, S. D., & Richstone, D. O. 1977, ApJ, 212, 311
White, S. D. M. 1976, MNRAS, 174, 19
White, S. D. M. 1977, Comm. Astrophy., 7, 95
White, S. D. M. 1983, MNRAS, 174, 19
Zhao, J-H., Burns, J. O., & Owen, F. N. 1989, AJ, 98, 64